ELSEVIER

Materials Science and Engineering A216 (1996) 80–90

MATERIALS SCIENCE & ENGINEERING A

Resistance-curve toughening in ductile/brittle layered structures: behavior in Nb/Nb_3Al laminates

D.R. Bloyer, K.T. Venkateswara Rao, R.O. Ritchie

Department of Materials Science and Mineral Engineering, University of California, Berkeley, CA 94720-1760, USA

Received 31 January 1996; revised 18 April 1996

Abstract

A study has been made of the fracture toughness and resistance-curve behavior of a laminate consisting of alternating layers of brittle Nb_3Al intermetallic and ductile Nb metal, using layer thicknesses of ~500 and 125 μm, respectively. Effective resistance-curve toughening of Nb_3Al was achieved in such a coarse-scale layered structure with only 20 vol.% of the Nb reinforcement phase. Specifically, the toughness of Nb_3Al was increased from ~1 MPa$\sqrt{m}$ to well over 20 MPa$\sqrt{m}$ (and as high as 70 MPa$\sqrt{m}$ in certain samples) after several millimeters of stable crack growth. These values are significantly greater than other Nb/Nb_3Al composites containing Nb as ~20 μm sized particulates or 1–2 μm thick Nb layers (in the form of a microlaminate), both containing at least 40 vol.% of the ductile phase. The source of such ductile-phase toughening was attributed to crack blunting at, and renucleation across, the ductile Nb layers, which in turn led to extensive bridging and plastic deformation within the Nb layers in the crack wake. Since the extent of crack trapping by the ductile layer and plastic deformation are limited by layer thickness, the present coarser-scale laminates tend to display better fracture resistance compared to composites with finer-scale ductile reinforcements.

Keywords: Fracture toughness; Resistance curve toughening

1. Introduction

Intermetallic alloys have generated increasing interest over the past decade as possible replacements for titanium- and nickel-based superalloys currently used in aerospace applications owing to their higher melting temperatures and lower densities, which provide improved specific creep strength for elevated temperature structures in high performance engines [1–3]. However, as most intermetallic compounds are brittle due to their ordered crystal structures, they generally suffer from poor room-temperature fracture resistance. An example of this is niobium aluminide, Nb_3Al; although it is one of the highest melting point aluminides with excellent creep resistance, it exhibits a fracture toughness, K_{Ic}, of only ~1 MPa$\sqrt{m}$ at ambient temperature. In an attempt to improve such poor intrinsic toughness, extrinsic toughening techniques that invoke crack-tip shielding mechanisms are often used in alloy design and microstructural development. Such mechanisms, which include crack bridging in composites and crack closure during fatigue crack growth, primarily act behind the crack tip and locally "shield" the crack from the far-field (applied) "driving force" [4,5]. Examples of materials toughened in this manner are several ceramic and intermetallic matrix composites that incorporate ductile or brittle reinforcements in the form of fibers, particulates, or laminates [1–3,6–19].

In the present study, we examine the fracture behavior of one such composite, Nb-reinforced Nb_3Al, where toughening is achieved through the incorporation of Nb layers. Niobium, being a refractory metal, was chosen because of its high-temperature properties and its ductile constitutive behavior, compared to Nb_3Al, at room temperature. Previous studies on this system have focused on the influence of Nb as ~20 μm sized particulates, dispersed in situ through powder metallurgy (P/M) techniques [6,7], or as ~1–2 μm thick layers to form a microlaminate by magnetron sputtering [8,9]. The current investigation examines the fracture toughness response in a model laminate consisting of coarse Nb layers in a Nb_3Al matrix, where the layer dimensions are in the hundreds of microns.

0921-5093/96/$15.00

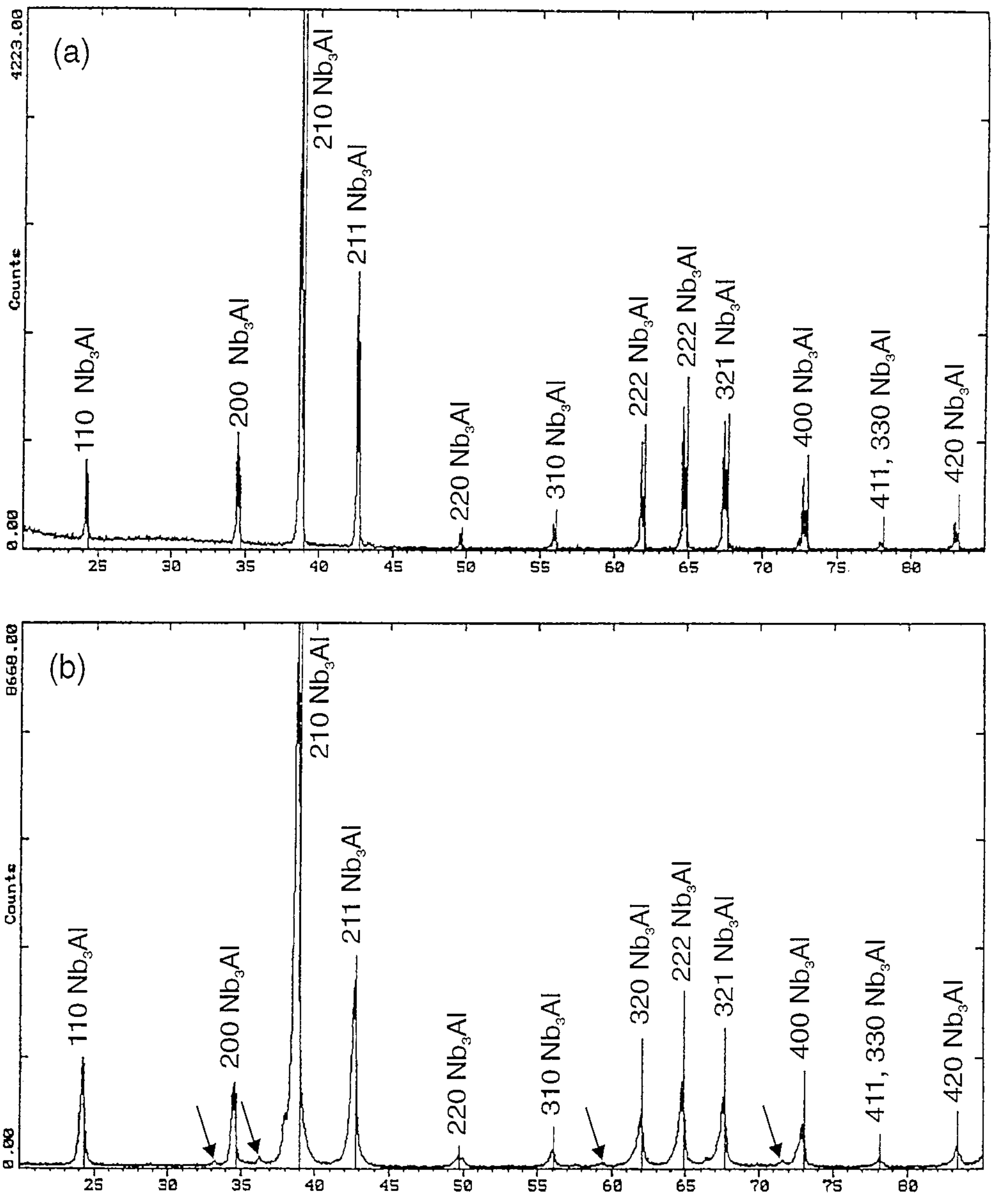

Fig. 1. X-ray diffraction patterns taken for (a) synthesized Nb_3Al powder and (b) hot-pressed Nb_3Al. Note the traces of Nb_2Al, as indicated by labeled peaks, in the hot-pressed condition.

2. Experimental procedures

Nb_3Al powder was prepared by reaction synthesis of elemental Nb (Cerac, 99.8%, -325 mesh) and Al (Valimet, 99.3%, -325 mesh) powders in the molar ratio 0.76 Nb–0.24 Al; the oxygen content of the Nb starting powder was 1670 ppm. Powders were mixed in a ball mill for approximately 0.5 h, and then heated in a helium atmosphere at 1400 °C for 4 h to enable the formation of Nb_3Al. The reacted powder was subsequently ball milled for approximately 0.5 h, and reheated to 1400 °C for an additional 4 h to complete the reaction. The Nb_3Al powder was ball milled again for 1 h, to achieve a fine particle size (mean particle size, ~ 20 μm), prior to use in composite fabrication. X-ray diffraction was used to verify the formation of Nb_3Al in the synthesized powder prior to hot pressing the Nb/Nb_3Al laminates; however, traces of Nb and Nb_2Al were sometimes observed (Fig. 1).

The laminates were prepared by sequentially cold pressing layers of Nb_3Al powder between 125 μm thick Nb foils (Rembar Co.) to yield ~ 20 vol.% ductile reinforcement. Cold compaction was performed in a graphite mold, followed by hot pressing in an argon atmosphere at 1680 °C under 37 MPa pressure for 40 min to give a dense ($> 98\%$ of theoretical density) composite cylinder. For this investigation, laminates consisting of 15 layers each of the metal and intermetallic phase were prepared. The resultant microstructure consisted of evenly spaced 500 μm thick layers of

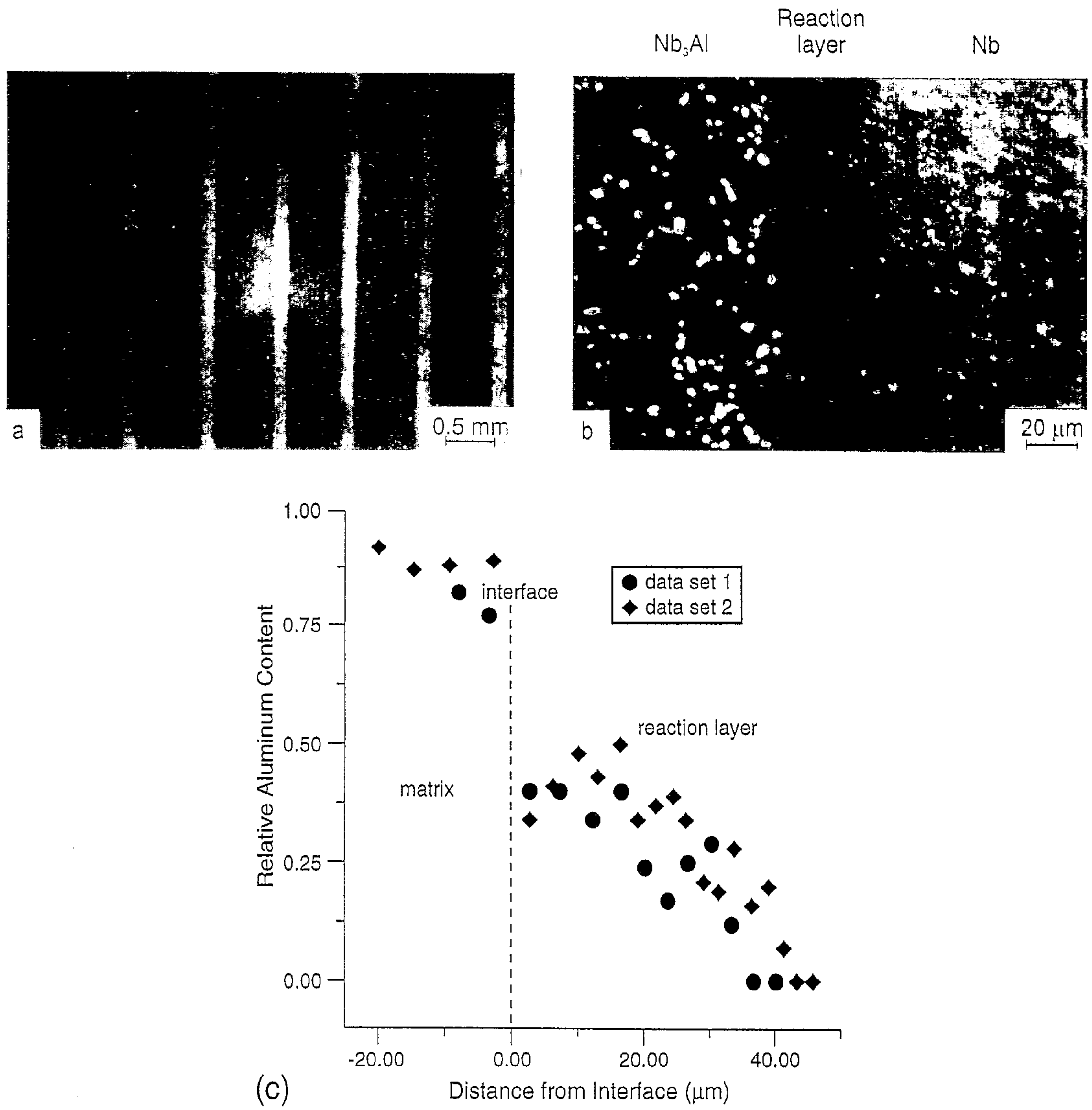

Fig. 2. (a) Macroscopic photograph showing the layered structure of the Nb/Nb_3Al laminate. (b) Magnified view of the interface between the Nb_3Al and the Nb depicting the reaction layer. (c) Relative aluminum content in the reaction layer, taken by standardless energy dispersive spectroscopy, showing an interdiffusion region of 30–40 μm.

Nb_3Al separated by 125 μm thick layers of Nb (Fig. 2(a)). A reaction zone, ~30 μm in thickness, formed between the layers during processing at 1680 °C (Fig. 2(b) and 2(c)), resulted in approximately 40% reduction in the Nb layer thickness.

The processed laminated cylinder was sectioned using electro-discharge machining into rectangular, single-edge notched SEN(B) beams in the 0° (C–L) orientation, where the crack grows perpendicular to the layers, i.e. "crack arrester" orientation. Beams were machined with lengths ranging from 35 to 40 mm, a thickness of $B = 3.5$ mm and a width of $W = 12.5$ mm. Initial notches were cut to depths of $\sim 0.2W$, and further extended by precracking in fatigue to a depth of $\sim 0.3W$. Testing was conducted in three-point bend loading with spans of 35–40 mm; one test was performed in four-point bending with inner and outer spans of 15.2 mm and 30.4 mm, respectively.

The fracture toughness of the laminate was examined by measuring the resistance-curve (or R-curve) behavior in terms of the stress intensity required for crack initiation and subsequent growth as a function of crack extension, Δa. R-curves were determined by manually loading specimens under displacement control at a nominal rate of 5–10 μm min^{-1} using an Instron 1350 servo-hydraulic test machine equipped with an 8500 digital controller. Fatigue pre-cracking aided in fracturing ductile layers that may have remained intact behind the crack tip prior to R-curve testing. Crack lengths were measured by indirect electrical potential methods using thin foil gauges bonded to the side of the specimen. Measurements were confirmed by direct observation using a high-resolution (Questar) telescope attached to a video camera. The video system allowed real time observation of the crack profile development and image-capturing capability to study crack/layer interactions. Following each crack advance, applied loads were reduced by 10–15% while relevant observations were recorded. Specimens were then reloaded to further extend the crack, and the process was repeated until the crack reached a crack length to width (a/W) ratio of ~ 0.8, or until final fracture ensued. After testing, profiles of crack paths, at both surface and mid-thickness locations, and fracture surfaces were examined using scanning electron microscopy and metallographic sectioning.

3. Results and discussion

3.1. Fracture toughness and R-curve behavior

R-curve behavior for the Nb/Nb_3Al laminate is shown in Fig. 3 and clearly illustrates the significantly higher fracture resistance of the composite compared to unreinforced Nb_3Al. The increase in toughness is apparent for crack initiation (i.e. as $\Delta a \rightarrow 0$) and particularly for crack growth. Cracking initiated in the laminate at ~ 9 $MPa\sqrt{m}$, and involved stable crack advance at progressively higher stress intensities exceeding 15–20 $MPa\sqrt{m}$, due to crack bridging by intact Nb layers in the crack wake; in contrast, the matrix failed catastrophically at K_{Ic} values of ~ 1 $MPa\sqrt{m}$. In one case, 5–6 mm of stable crack growth was seen at stress intensity levels as high as 70 $MPa\sqrt{m}$ before final failure of the sample.

The present Nb/Nb_3Al laminate, with only 20 vol.% of the Nb reinforcement, exhibits considerably higher toughness than that reported for in-situ Nb/Nb_3Al composites [7] with 40 vol.% of (~ 20 µm size) Nb particulates or microlaminates containing 40–50 vol.% of (~ 1 2 µm thick) Nb layers (Fig. 3(b)). Compared to the particulate Nb/Nb_3Al composite where the initiation and steady-state ("plateau") toughnesses were ~ 1 and 6 $MPa\sqrt{m}$, respectively [7], crack growth in microlaminates initiates at about 6 $MPa\sqrt{m}$ and increases to a maximum value of ~ 10 $MPa\sqrt{m}$ after ~ 200 µm of crack extension[9]. In contrast, current results on Nb/Nb_3Al macrolaminates show quasi-static crack growth only above ~ 9 $MPa\sqrt{m}$, which remains stable up to stress intensities approaching 70 $MPa\sqrt{m}$. Two points are noteworthy. First, the comparison between microparticulate and microlaminate Nb/Nb_3Al composites demonstrates the ability of oriented, high-aspect ratio reinforcements (i.e. fibers and laminates) in imparting better damage tolerance to materials, similar to observations made in $Nb/MoSi_2$ composites [10–12]. Secondly, it appears that layered reinforcements with coarse dimensions (125 µm) are far more effective than fine (1–2 µm) layers in enhancing the fracture resistance of ductile-phase toughened Nb/Nb_3Al composites, despite the higher reinforcement content in the micron-scale laminates.

It must be pointed out that a direct comparison of current results with reported behavior in Nb/Nb_3Al microlaminates [9] may be somewhat clouded by the fact that the latter were tested in the "crack divider" (C–L) orientation (where the crack plane is normal to the plane of layers, but the crack advances through all the layers simultaneously). However, studies on TiNb/TiAl laminates, with equivalent reinforcement dimensions and content, suggest the role of orientation on overall (plateau) toughness to be small, although crack divider configurations tend to exhibit lower initiation toughness compared to the arrester [13,14]. Moreover, the orientation difference is expected to be partially offset by the higher amount of Nb phase in the microlaminates. In essence, the present results highlight the marked efficiency of adding a small volume fraction of coarse, layered reinforcements on ductile-phase toughening, and hence, in improving the fracture resistance of brittle Nb_3Al composites.

The rapid increase in toughness in the coarse-laminated composite, especially for crack extensions beyond 3 mm where cracking occurs at stress intensities above 30 $MPa\sqrt{m}$ to levels as high as 70 $MPa\sqrt{m}$, can be attributed to large-scale shielding. Such effects become prominent when the size of the shielding zone in the crack wake becomes comparable to specimen dimensions, such as the length of the crack or uncracked ligament. As noted below, such shielding effects in the present composite arise from bridging by the ductile Nb layers. Indeed, compared to R-curves that display a plateau, such as those seen in particulate and microlayered Nb/Nb_3Al composites, the increasing slope and positive curvature of the R-curve with increasing Δa for the macrolaminate (Fig. 3) are common indications that large-scale bridging conditions prevail during crack propagation.

3.2. Crack/particle interactions

Metallographic sections of the crack path and scanning electron micrographs of fracture surfaces indicate that the higher toughness in the present Nb/Nb_3Al laminates can be attributed to the greater effectiveness of coarse Nb layers in promoting crack-reinforcement interception and resultant crack bridging. For example, as shown in Fig. 4(a), after roughly 6 mm of crack growth, the macroscopic crack-path morphology shows a single dominant crack with limited crack branching and five unbroken Nb layers behind the crack tip, thereby creating a bridging zone on the order of 3 mm in the crack wake. While these represent observations made on the surface of the specimen, a similar profile

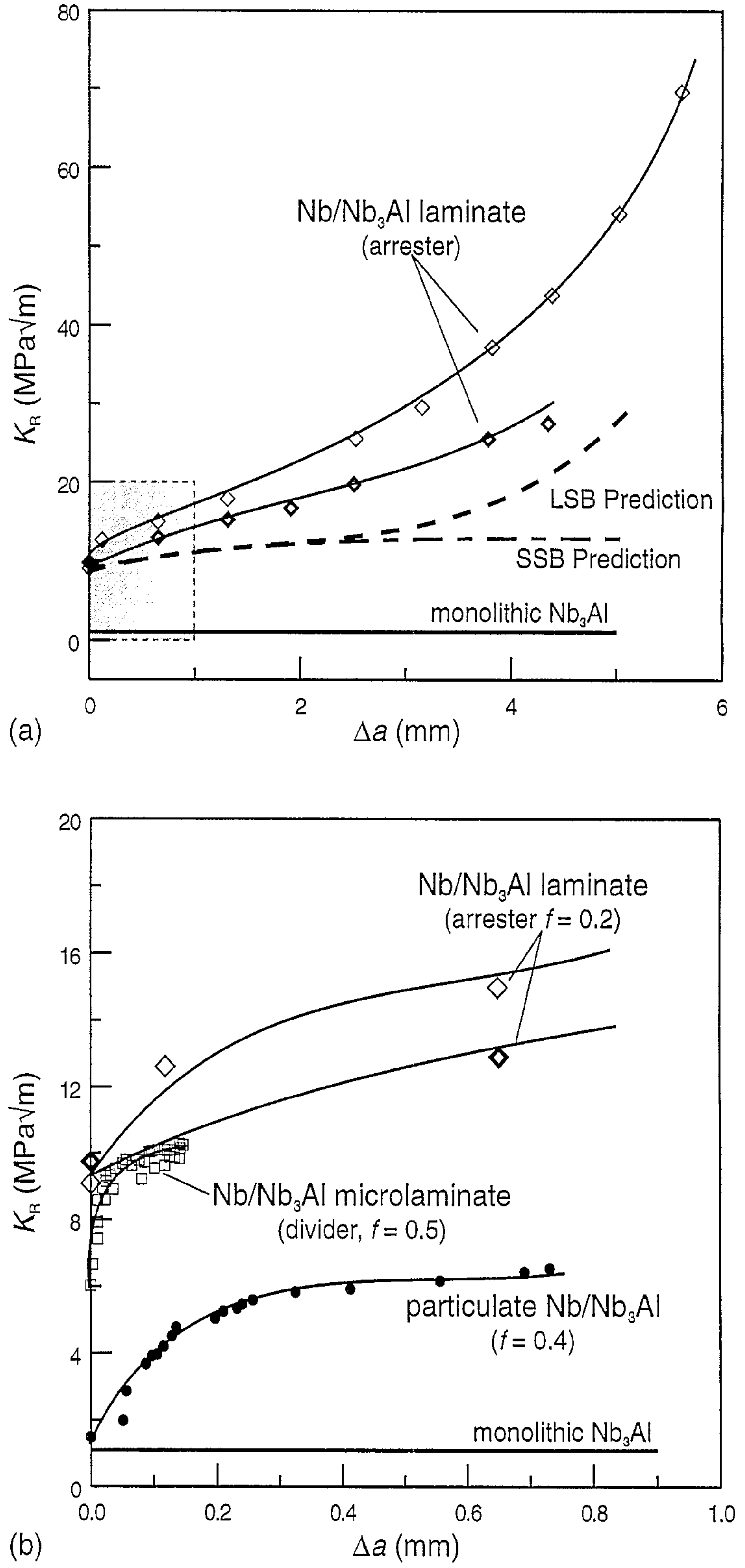

Fig. 3. *R*-curve behavior for the present Nb/Nb$_3$Al laminates in the arrester orientation, compared to (a) monolithic Nb$_3$Al, (b) in-situ Nb$_3$Al composites reinforced with Nb particulate [6] and Nb/Nb$_3$Al microlaminates [9]. Predictions for the *R*-curve of the Nb/Nb$_3$Al laminates, based on small-scale bridging (SSB) and large-scale bridging (LSB) models, are also shown in (a). Shaded region of (a) is magnified in (b).

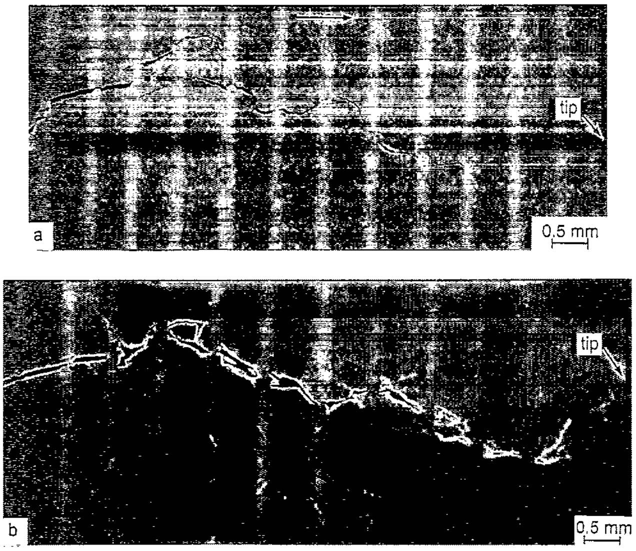

Fig. 4. Micrographs of a cracked Nb/Nb_3Al laminate, showing the profile of the crack path, (a) taken at the surface, and (b) interior, at the center of the beam thickness. Arrow indicates direction of crack growth.

taken at the center of the beam, again perpendicular to the fracture surface (Fig. 4(b)), reveals that the zone of bridging can extend as far back as ten Nb layers, or roughly 5 mm behind the crack tip. Not all Nb layers in this zone are intact and act as bridges; in fact, the specific bridging layers vary between profiles. This suggests that crack bridging from Nb layers may not be continuous across the crack front, i.e. through the specimen thickness.

Higher magnification images in Figs. 5 and 6 reveal the details of crack/layer interactions that lead to the formation of a bridging zone of unbroken Nb layers. A typical sequence of events indicative of the local failure process is described below.

- Upon loading, the crack in the Nb_3Al matrix impinges on the Nb reinforcement and arrests in the reaction layer. No debonding along the Nb/Nb_3Al interface is seen.
- The crack, then penetrates the reaction layer on the leading side of the Nb layer.
- On further loading, the crack renucleates in the Nb_3Al matrix on the other side of the Nb layer some distance above or below the crack plane, and leaves the Nb layer intact. The out-of-plane offset distance is less than, or equal to, the layer thickness.
- The crack, then penetrates back through the reaction layer on the trailing side of the Nb layer and blunts, thereby causing the crack to be bridged by the surviving Nb layer.
- At larger crack-opening displacements, intense shear bands appear in the ductile Nb layer concurrent with the onset of extensive plastic deformation in the Nb, leading to final failure of the Nb layer.

The initial steps are evident in Fig. 5(a), where the crack has failed to penetrate the reaction layer of the Nb reinforcement immediately behind the crack tip (layer 1), although there is penetration into the reaction layer on both sides in the next reinforcement (layer 2). The through-thickness nature of this phenomenon was verified by taking a section through the center of the specimen to expose the internal crack profile; Fig. 5(b) clearly indicates that the crack exhibits equivalent response on the surface and in the interior. Direct evidence of crack renucleation in the Nb_3Al matrix and "retro-penetration" into the reaction layer can also be seen on the fracture surfaces of regions surrounding the Nb layer. Fig. 5(c) shows a ruptured bridge where the radial spreading of river markings on cleavage facets in the reaction layer in opposite directions clearly indicates crack advance into Nb from both sides of the layer. These events recur as the crack advances across several Nb layers leaving them intact and consequently lead to the formation of a large ($\sim$ 3–5 mm) bridging zone in the crack wake. Following large crack openings, extensive plastic deformation of the ductile Nb bridges in the form of shear bands is seen (Fig. 6(a)), which results in the eventual failure of the Nb layer.

Although this sequence of events leading to toughening from crack bridging by unbroken Nb layers in the crack wake was typical of local crack/layer interactions, other cracking patterns were also noted. For example, the crack sometimes penetrated the reaction layer upon first encountering a Nb layer; on other occasions, it would branch on one or both sides of the Nb layer (Fig. 5(a) and (b), and Fig. 6(a)–(c)). The branching usually occurred in the matrix near the Nb/Nb_3Al interface, but not necessarily at the interface; the branches then linked up to form a single dominant crack as the crack progressed across the specimen. Apart from branching, renucleation of multiple cracks ahead of the Nb layer, above and below the main crack plane, was also seen (Fig. 5(a) and Fig. 6(c)); eventually, one of them became dominant while the rest remained dormant (Fig. 4). No crack growth was apparent along the Nb/Nb_3Al interface. However, both cracking modes, namely crack branching and multiple cracking in the Nb_3Al matrix, resulted in "effective debonding" at the Nb/Nb_3Al interface, thereby promoting ductile failure of the Nb layer (Fig. 6(a)), as discussed below. In addition to debonding considerations, out-of-plane crack renucleation across a layer (as indicated in Fig. 6(b), at distances comparable to the layer thickness), can also increase the shielding effectiveness of the bridging layer, and enhance toughness over the simple necking-type rupture usually observed in laminated composites [15]. Finally, crack deflection, which was observed on a macroscopic scale with deflection angles ranging between 10 and 30° (Fig.

4), can further provide some contribution to toughening of the Nb/Nb_3Al laminate.

3.3. Fractography and fracture mechanisms

The Nb_3Al matrix and reaction layer exhibit transgranular cleavage fracture, whereas the reinforcing Nb layers display features of both ductile and brittle fracture (Fig. 7). Three distinct failure modes were observed in the Nb layers, namely, brittle cleavage-like failure (Fig. 7(a)), ductile microvoid coalescence (Fig. 7(b)), and a mixture of the two (Fig. 7(c)), with the incidence of ductile vs. brittle failure depending upon the degree of matrix cracking at or near the Nb/Nb_3Al interface. Where near-interfacial cracking occurred in the matrix (Fig. 7(b)), microvoid coalescence prevailed, presumably because the cracks relieve constraint in the Nb layer, thereby reducing the probability of brittle fracture. Conversely, when no interfacial cracking appeared, the constraint imposed on the Nb layer is believed to promote cleavage fracture. A similar re-

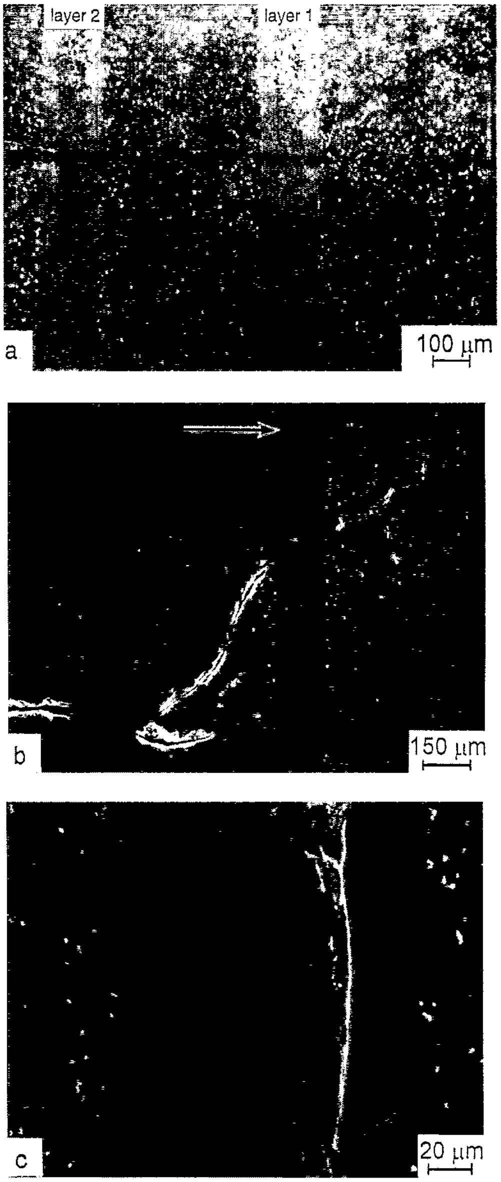

Fig. 5. Cracking sequence in the Nb/Nb_3Al laminate. (a) Surface crack profile shows that Nb layer immediately behind the crack tip has no reaction layer penetration, whereas the second layer behind the tip shows penetration into both sides of the Nb layer. (b) Similar behavior can be seen in the interior profile. (c) Markings on cleavage planes in the reaction layer also suggest that the crack penetrated into the layer from both sides of the reinforcement. Arrow indicates direction of crack growth.

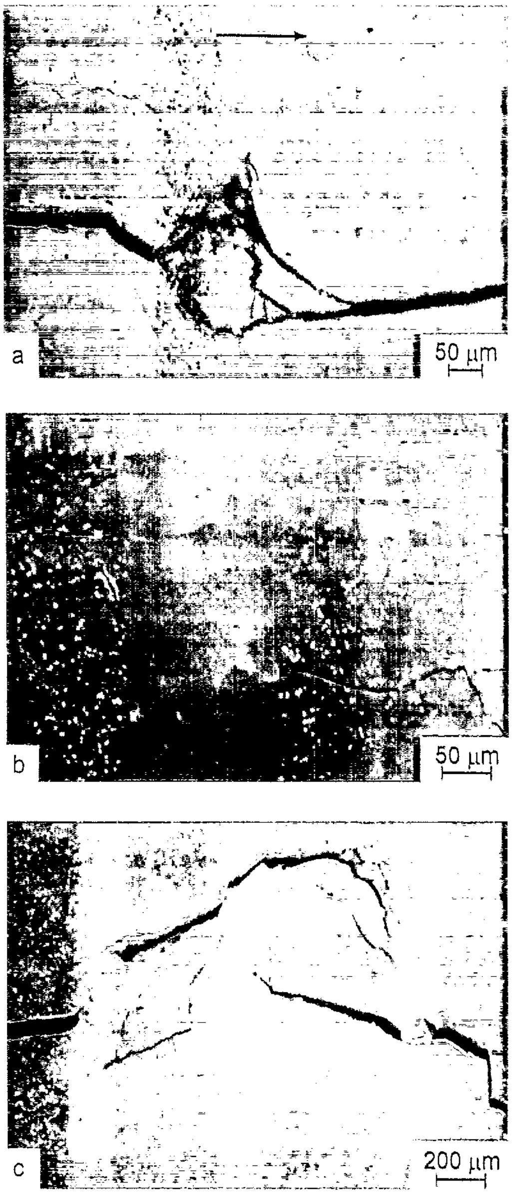

Fig. 6. Cracking in the Nb_3Al matrix near the Nb reinforcing layers in the Nb/Nb_3Al laminates. (a) Intense shear band formation related to the large crack opening and crack branching in the matrix. (b) Crack branching and out-of-plane crack renucleation across the Nb layer. (c) Significant crack deflection, uncracked ligament bridging, out-of-plane renucleation and crack branching. Arrow indicates direction of crack growth.

sponse has been reported in other ductile-phase reinforced systems, including lead/glass [15,16], Nb/Nb_5Si_3 [17] and $Nb/MoSi_2$ [11]. However, interfacial cracking that relaxes constraint in Nb/Nb_3Al laminates is not associated with decohesion along the Nb/Nb_3Al interface, but results from severe crack branching and multiple cracking in the Nb_3Al matrix surrounding the Nb layers (Figs. 5 and 6). It should be noted, however, that although cleavage fracture in body-centered cubic materials, such as Nb, is promoted by triaxial constraint which acts to restrict plastic stretching of the metal, interstitial impurities (most likely Al in this case) and

Fig. 7. Mechanisms of failure of the Nb reinforcement layer in the Nb/Nb_3Al laminates, showing (a) cleavage fracture, (b) secondary cracking near the interface and additional plastic stretching in the matrix to cause microvoid coalescence in the Nb reinforcement layer, and (c) mixed cleavage and ductile fracture. Arrow indicates the direction of crack growth.

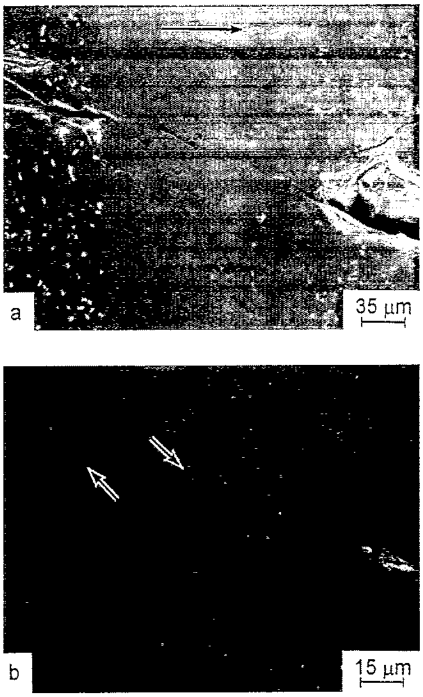

Fig. 8. Crack profile in metallographically sectioned Nb/Nb_3Al laminate specimen, showing (a) angled parallel cracking in Nb layer with (b) enlargement of the bridging ligament between microcracks in layer. Arrow indicates direction of crack growth.

the large grain size of the Nb layer (due to grain growth during processing at high temperatures) may also be contributing factors.

Where the Nb layers fail by a combination of both mechanisms, the fracture surfaces (Fig. 7(c)) show regions of void coalescence separating cleavage facets that penetrate into and out of the crack plane. Fig. 8(a) and 8(b) shows a profile taken at the mid-thickness location of a sample where a set of angled parallel cracks in an intact reinforcing layer; i.e. discrete bridging by Nb ligaments within a single layer. As these ligaments rupture, they appear to form shear-like dimpled fracture regions exhibiting void coalescence, connecting the two offset planes of cleavage facets. Ductile shear failures of this nature have been shown to greatly enhance work of rupture in lead/glass laminates [15], with increases by a factor of seven being reported, and are expected to also contribute towards the improved fracture resistance of Nb/Nb_3Al composites.

3.4. Models for toughening

The principle behind ductile-phase reinforcement of brittle materials is to promote crack–particle interaction, to generate a zone of bridging ligaments that provide closure tractions in the wake that restrict crack opening, and to utilize plastic deformation of the ductile phase to resist failure. Most models for such ductile-phase toughening pertain to small-scale bridging conditions, where the bridging zone is small relative to crack length and remaining uncracked ligament in the sample. However, for the laminates examined in this study, it is apparent that the bridging zone length approaches the size of these characteristic dimensions, such that conditions of large-scale bridging prevail and the R-curve then depends on specimen geometry. Accordingly, both small-scale and large-scale bridging models were used to evaluate the role of layered Nb reinforcements on the fracture toughness of Nb/Nb_3Al laminates, as discussed below.

3.4.1. Small-scale bridging

Bridging models typically require two experimental parameters, the stress-displacement function for the constrained reinforcement in the matrix, $\sigma_c(u)$, and the critical displacement at the failure of this reinforcement, u_c. These parameters can be used to estimate the non-dimensional work of rupture for the reinforcement, χ, given by [16]:

$$\chi = \int_0^{u_c} \frac{\sigma_c(u)\,du}{\sigma_o \cdot t} \tag{1}$$

where σ_o is the flow stress (average of the yield and ultimate strength) and t is the characteristic cross-section, respectively, of the reinforcement. For a volume fraction, f, the increase in fracture energy is then given by [16]:

$$\Delta G_c = f\sigma_o t\chi \tag{2}$$

For conditions of small-scale bridging, the steady state toughness, G_{ss}, can be obtained from:

$$G_{ss} = G_o + \Delta G_c \tag{3}$$

where G_o is the strain energy release rate for crack initiation in the composite. Note that although G_o is often taken as the matrix toughness, it can exceed this value when crack trapping by the reinforcement phase requires renucleation of the crack across the phase. Eq. (3) can be rewritten in terms of stress intensities as [18]:

$$K_{ss} = \sqrt{K_o^2 + E' f\sigma_o t\chi} \tag{4}$$

where K_{ss} is the steady-state (or plateau) toughness, and K_o is the crack-initiation toughness.

To evaluate Eq. (4), we note that values of χ between 1.3 and 2.5 [19,12] have been reported for Nb/TiAl and $Nb/MoSi_2$ laminates of similar microstructural scale; as these values were influenced by small amounts of debonding, a conservative value of $\chi \sim 1.3$ will be assumed here. Because of the presence of the reaction layer, the effective volume f and half layer thickness t of the Nb phase are reduced; these values were estimated to be $f \sim 0.14$ and $t \sim 37.5$ μm. Using $K_o \sim 9$ MPa$\sqrt{m}$ (Fig. 3), a plane-strain composite modulus, $E' = 142$ GPa (assuming $E_{composite} = 129$ GPa and $\nu \sim 0.3$), and the flow stress of Nb, $\sigma_o \sim 245$ MPa [20], Eq. (4) predicts a steady-state toughness of ~ 18 MPa$\sqrt{m}$, which is slightly below the measured plateau toughness value (Fig. 3(a)).

An alternative model, developed originally for particle-reinforced composites [21,22], treats the bridges as rigid plastic springs which provide a uniform traction field in the wake. The far-field mode I stress intensity at steady state, K_{ss}, is computed by superposition of the crack-tip stress intensity, K_o, and the shielding stress intensity imparted by the tractions, ΔK_c, given as:

$$\Delta K_c = \frac{2}{\sqrt{\pi a}} \int_0^L \sigma(x) F\left(\frac{x}{a}, \frac{a}{W}\right) dx \tag{5}$$

where a is the crack length, x is the distance behind the crack tip, W is the specimen width, L is the bridging zone length, $\sigma(x)$ is a stress function describing the tractions in the wake, and the geometric weight function F is given in Refs. [21–23]. Note that if small-scale bridging conditions dominate, F simplifies to $(a/2x)^{\frac{1}{2}}$ [21,22]. By equating K_o to the initiation toughness, and traction function $\sigma(x) = f\sigma_o$ (flow stress times the area fraction of reinforcements intersecting the crack plane), the composite toughness at steady state can be expressed as:

$$K_{ss} = K_o + 2f\sigma_o\sqrt{\frac{2L}{\pi}} \tag{6}$$

Taking the bridging zone to be 5 mm, Eq. (6) predicts a toughening increment of ~ 4 MPa$\sqrt{m}$ which yields a predicted steady-state toughness of ~ 13 MPa$\sqrt{m}$. This model, however, underestimates the values measured for the Nb/Nb_3Al laminate as it does not account for additional effects from crack branching, deflection and multiple cracking observed during crack growth.

Despite the apparent agreement of the small-scale bridging models, several other factors should be recognized. These include (i) the possible elevation in the yield strength of the Nb phase due to solid-solution strengthening, akin to the impurity hardening of Nb due to Si diffusion in $Nb/MoSi_2$ composites [17,24], and (ii) the variation in this yield strength due to changes in the local strain rate. In general though, small-scale bridging models will underpredict the fracture toughness response of coarse-laminated composites measured using small samples as the bridging zone length is comparable to the characteristic dimensions of the sample. Accordingly, large-scale bridging models should provide a better description of their R-curve behavior.

3.4.2. Large-scale bridging

For large-scale bridging conditions, Eq. (5) can be used directly, although predictions will be complicated by the fact that the R-curve is also dependent on specimen geometry. A rigorous modeling approach requires the use of the exact stress-displacement function

($\sigma_c(u)$) and crack-opening profile ($u(x)$) for the specific geometry [13]. However, assuming uniform tractions as before ($\sigma(x) = f\sigma_o$) and weight functions, F, developed for single-edge notched samples [22,23], a simple estimate for the R-curve under large-scale bridging conditions can be obtained by integrating Eq. (5) at various crack-growth increments and superimposing the toughening increment, ΔK_c, over the matrix crack-tip stress intensity K_o. Predicted results for the coarse Nb/Nb_3Al laminates tested in this study, up to a final bridging zone length of 5 mm, are shown in Fig. 4(a). The modeling still underpredicts the R-curve data as the calculations are not iterative to include the development of the crack-opening profile and resultant tractions, and do not consider the role of other shielding mechanisms. However, the predicted behavior is consistent with the observed trend for crack-growth toughness (increasing slope and positive curvature) under large-scale bridging conditions.

4. Concluding remarks

Present results combined with previous studies on ductile-phase toughened composites [6–18] demonstrate the marked efficiency of aligned, high aspect-ratio reinforcements, especially layered reinforcements, in enhancing the fracture resistance of brittle intermetallics. Such composite microstructures are most effective in promoting crack path interception and realizing the benefits of shielding from crack bridging and plastic deformation within the ductile phase. Additionally, it is clear that coarse-laminated microstructures, with considerably lower reinforcement content, exhibit remarkably higher toughness compared to finer scale laminates. Since crack-initiation toughness is governed primarily by the renucleation stress intensity, which is expected to be roughly proportional to square root of layer thickness, thicker metal layers redistribute the crack-tip stress singularity over greater distances ahead of the crack tip and more effectively lower the crack driving force compared to fine-scale reinforcements.

Plasticity and stress-displacement behavior of the ductile metal layer influence the crack-growth toughness and subsequent development of the R-curve. For nominally similar interface properties and failure mechanisms (using either fine or coarse-scale reinforcements), the volume of metal undergoing plastic deformation will be greater in the coarse compared to fine-scale laminates because of a lower triaxial constraint. Correspondingly, the critical displacement (or strain) to failure is higher, which is responsible for the large bridging zone and increased crack-growth toughness in the coarse-layered microstructures. The role of renucleation and plasticity is limited in fine-scale ductile-phase microstructures to bridging-zone dimensions of ≤ 400 μm, such that the improvement in fracture resistance, in a engineering sense, is measured as an overall increase in crack-initiation toughness. In contrast, macrolaminates yield large increases in crack-initiation and crack-growth toughnesses due to crack trapping/renucleation and yielding in the metal layer, and their behavior is influenced by large-scale bridging. From this perspective, an appropriate dimension for microstructural design of ductile/brittle laminates with optimal fracture resistance would be a layer thickness equivalent to the maximum plastic-zone size under plane stress conditions. This suggests that highly refined microstructures below these dimensions, such as nanocomposites or nanostructured materials, may have limited structural use for engineering applications, at least where damage tolerance is required.

5. Conclusions

Based on a study of the fracture toughness and resistance-curve behavior of ductile Nb-reinforced Nb_3Al intermetallic matrix laminates, the following conclusions can be made.

(1) Effective resistance-curve toughening of Nb_3Al was achieved through reinforcement with ~ 125 μm thick Nb layers to form of a coarse Nb/Nb_3Al laminate. With only 20 vol.% Nb, the toughness of Nb_3Al was increased from ~ 1 $MPa\sqrt{m}$ to well over 20 $MPa\sqrt{m}$ (and as high as ~ 70 $MPa\sqrt{m}$ in one sample under large-scale bridging conditions) after several millimeters of stable crack extension.

(2) The toughness of coarse, 125 μm thick Nb/Nb_3Al laminates was also significantly greater than Nb/Nb_3Al composites containing ~ 20 μm thick Nb particulate or 1–2 μm thick Nb layers in the form of a microlaminate with reinforcement phase fractions of 40 vol.% or higher.

(3) Toughening in the coarse Nb/Nb_3Al laminates was attributed to shielding from ductile-phase bridging. Specifically, crack blunting at ductile Nb layers and renucleation in the matrix ahead of the layer resulted in the formation of intact Nb ligaments in the crack wake. The coarse Nb layers elevate the renucleation stress intensity and also result in larger bridging zones, both factors that promote toughening. Moreover, since the extent of plasticity in the Nb layer is limited by the layer thickness, the larger zones of plastically deformed material in the thicker laminates provide a greater contribution to the toughness.

(4) The Nb phase failed by three mechanisms, namely brittle cleavage fracture, ductile microvoid coalescence, and a combination of the two. The two latter processes provided significant energy dissipation from plasticity and are believed to enhance crack-

growth toughness. Near-interface cracking parallel to, and microcracking within, the Nb reinforcing layers appeared to relieve constraint and promote plastic deformation within the Nb phase.

Acknowledgements

This work was supported by the Air Force Office of Scientific Research under the AASERT Program (Grant No. F49620-93-1-0441) as a supplement to Grant No. F49620-93-1-0107, with Dr. C.H. Ward as Program Manager. Thanks are due to Dr. Ward for his continued support, to Dr. B.J. Dalgleish for his help with materials processing, and to Prof. L.C. DeJonghe for the use of his hot-pressing facilities.

References

[1] R.L. Fleischer, in C.T. Liu et al. (eds.), High Temperature Ordered Intermetallic Alloys III, *Mater. Res. Soc. Symp. Proc.*, *133* (1989) 305.
[2] D.L. Anton and D.M. Shah, in C.T. Liu et al. (eds.), High Temperature Ordered Intermetallic Alloys III, *Mater. Res. Soc. Symp. Proc.*, *133* (1989) 361.
[3] D.L. Anton and D.M. Shah, in D.L. Anton et al. (eds.), Intermetallic Matrix Composites, *Mater. Res. Soc. Symp. Proc.*, *194* (1990) 45.
[4] A.G. Evans, *J. Am. Ceram. Soc.*, *73* (1990) 187.
[5] R.O. Ritchie, *Mater. Sci. Eng.*, *A103* (1988) 15.
[6] L. Murugesh, K.T. Venkateswara Rao and R.O. Ritchie, *Scr. Metall. Mater.*, *41* (1993) 1107.
[7] C.D. Bencher, A. Sakaida, K.T. Venkateswara Rao and R. O. Ritchie, *Metall. Mater. Trans. A*, *26* (1995) 2027.
[8] H.C. Cao, J.P.A. Löfvander, A.G. Evans and R.G. Rowe, *Mater. Sci. Eng. A*, *A185* (1994) 87.
[9] R.G. Rowe, D.W. Skelly, M. Larsen, J. Heathcote, G. Lucas and G.R. Odette, in C.L. Briant, J.J. Petrovic, B.P. Bewlay, A.K. Vasudévan and H.A. Lipsitt (eds.), High Temperature Silicides and Refractory Metals, *Mater. Res. Soc. Symp. Proc.*, *322* (1994) 461.
[10] K.T. Venkateswara Rao and R.O. Ritchie, in W.O. Soboyejo, T.S. Srivatsan and D.L. Davidson (eds.), *Fatigue and Fracture of Ordered Intermetallic Materials I*, The Minerals, Metals and Materials Society, Warrendale, PA, 1994, p. 3.
[11] K.T. Venkateswara Rao, W.O. Soboyejo and R.O. Ritchie, *Metall. Trans. A*, *23A* (1992) 2249.
[12] K. Badrinarayanan, A.L. McKelvey, K.T. Venkateswara Rao and R.O. Ritchie, *Metall. Mater.Trans. A*, *28A* (1996) in press.
[13] G.R. Odette, B.L. Chao, J.W. Sheckhard and G.E. Lucas, *Acta Metall. Mater.*, *40* (1992) 2381.
[14] K.T. Venkateswara Rao, G.R. Odette and R.O. Ritchie, *Acta Metall. Mater.*, *42* (1994) 893.
[15] M. Bannister and M.F. Ashby, *Acta Metall. Mater.*, *39* (1991) 2575.
[16] M.F. Ashby, F.J. Blunt and M. Bannister, *Acta Metall. Mater.*, *37* (1989) 1847.
[17] J. Kajuch, J.D. Rigney and J.J. Lewandowski, *Mater. Sci. Eng.*, *A155* (1992) 59.
[18] K.T. Venkateswara Rao, G.R. Odette and R.O. Ritchie, *Acta Metall. Mater.*, *40* (1992) 353.
[19] H.E. Dève, A.G. Evans, G.R. Odette, R. Mehrabian, M.L. Emiliani and R.J. Hecht, *Acta Metall. Mater.*, *38* (1990) 1491.
[20] *ASM Metals Handbook*, 10th edn., Vol. 2, ASM International, Materials Park, OH, 1994, p. 559.
[21] B. Budiansky, J.C. Amazigo and A.G. Evans, *J. Mech. Phys. Solids*, *36* (1988) 167.
[22] F. Zok and C.L. Hom, *Acta Metall. Mater.*, *38* (1990) 1895.
[23] H. Tada, P.C. Paris and G.R. Irwin, *Stress Analysis of Cracks Handbook*, Del Research Corp./Paris Publ., St. Louis, MO, 1985.
[24] J. Kajuch, J. Short and J.J. Lewandowski, *Acta Metall. Mater.*, *43* (1995) 1955.